Article

Crystal OH mediating pathway for hydrogen peroxide production via two-electron water oxidation in non-carbonate electrolytes

Ruilin Wang[1], Hao Luo[1], Chengyu Duan[1], Huimin Liu[1], Mengdi Sun[1], Quan Zhou[1], Zheshun Ou[1], Yinglong Lu[1], Guanghui Luo[1], Jimmy C. Yu [2] & Zhuofeng Hu [1] ✉

Water oxidation presents a promising avenue for hydrogen peroxide (H_2O_2) production. However, the reliance on alkaline bicarbonate electrolytes as an intermediate has limitations, such as H_2O_2 decomposition and a narrow pH effectiveness range (7–9), restricting its utility across wider pH ranges. This study unveils a crystal OH mediating pathway that stabilizes SO_4OH* as a crucial intermediate. Basic copper carbonate ($Cu_2(OH)_2CO_3$) tablets, commonly found on cultural relics, exhibit the capability to generate H_2O_2 in neutral or acidic non-bicarbonate electrolytes. By leveraging this crystal OH mediating strategy, considerable H_2O_2 production in Na_2SO_4 electrolytes is achievable. Notably, the H_2O_2 production rate can reach 64.35 μmol h^{-1} at 3.4 V vs. RHE in a 50 mL 0.5 M Na_2SO_4 electrolyte. This research underscores the importance of crystal part in catalyst in catalyzing the 2e$^-$ water oxidation reaction, offering valuable insights for future investigations.

Hydrogen peroxide is a green energy substance that has garnered attention in various fields, including chemical manufacturing[1], biological and medical engineering[2,3], energy technology, and environmental remediation[3–5]. The traditional method of synthesizing H_2O_2 poses safety risks and requires large-scale infrastructure, resulting in energy waste and the need for H_2O_2 purification[4,6,7]. In-situ production of hydrogen peroxide, particularly through electrocatalytic methods, is a promising alternative due to its safe operation, ambient reaction conditions, on-demand production, and availability of inexpensive raw materials[8,9].

Electrocatalytic synthesis of hydrogen peroxide can be achieved by two kinds of pathways: two-electron cathode oxygen reduction reaction (2e$^-$ ORR) and two-electron anodic water oxidation reaction (2e$^-$ WOR). 2e$^-$ ORR pathway has been widely studied[10–14]. However, this method requires oxygen as a raw material, and a pumping device is unavoidably required during the entire reaction process because of the low solubility (~8 mg L^{-1} at 25 °C, 1 atm) and slow diffusion (2.1×10^{-5} cm^{-2} s^{-1}) of oxygen in the water, leading to high energy consumption and low oxygen utilization efficiency (<1%)[12]. By contrast, 2e$^-$ WOR does not require oxygen gas and is not limited by low solubility and slow diffusion of oxygen gas, making this method suitable in an oxygen-deficient environment. Moreover, the green energy of hydrogen (H_2) can be obtained simultaneously in the water electro-decomposition process (Eq. (1)).

$$H_2O \rightarrow O_2 + H_2 \uparrow \qquad (1)$$

At present, the most frequently used electrolyte in H_2O_2 electro-synthesis through 2e- WOR are $KHCO_3$ solution and K_2CO_3[15–20]. Gill et al. reported the role of bicarbonate-based electrolytes in the production of hydrogen peroxide through water oxidation. Specifically, HCO_3^- is oxidized to HCO_4^- or $C_2O_6^{2-}$ intermediates at the anode, and these intermediates oxidize water to hydrogen peroxide and then change back to HCO_3^- simultaneously[21,22]. Nadar et al. found that $BiVO_4$ with different index planes has different water oxidation performance to produce hydrogen peroxide. $BiVO_4$ with high-index planes is more favorable for the adsorption of HCO_3^- and thus favors the following

[1]School of Environmental Science and Engineering, Guangdong Provincial Key Laboratory of Environmental Pollution Control and Remediation Technology, Sun Yat-sen University, Guangzhou 510006, China. [2]Department of chemistry, The Chinese University of Hong Kong, Hong Kong, China. ✉ e-mail: huzhf8@mail.sysu.edu.cn

synthesis of hydrogen peroxide[23]. Hence, bicarbonate is beneficial to H_2O_2 generation.

However, bicarbonate-based electrolytes also suffer from two disadvantages. Firstly, it leads to the decomposition of hydrogen peroxide molecules leading to low hydrogen peroxide generation efficiency[23]. Jawad et al. demonstrated that bicarbonate consumes hydrogen peroxide. Specifically, bicarbonate can react with ·OH to generate water and ·CO_3^- radicals, and react with hydrogen peroxide to generate water and HCO_4^{-} [24]. Sablas et al. believe that both carbonate and bicarbonate can react with hydroxyl radicals to form ·CO_3^-. ·CO_3^- consumes hydrogen peroxide to form bicarbonate and $HO_2^·$, and $HO_2^·$ can react with ·CO_3^- to form carbonate[25]. That is, the presence of carbonate or bicarbonate decomposes the generated hydrogen peroxide. We have also proved that hydrogen peroxide cannot exist stably at ambient in the presence of bicarbonate even without applied bias. Specifically, the concentration of 1 mM hydrogen peroxide in 2 M $KHCO_3$ solution will decrease by 90% after 9 h. Second, bicarbonate is more soluble in the pH range of 7.0 − 9.0. However, if the pH is greater than 9, it will become carbonate with lower solubility[24].

Besides, another problem is that some applications of hydrogen peroxide in the environmental field require an acidic to neutral initial pH, but carbonates are often alkaline. Cao et al. show that effective degradation of tetracycline via H_2O_2 needs in a pH range of 3−7[26]. Fu et al. demonstrated that the pH value of tetracycline degradation by active H_2O_2 is 6[27]. Wang et al. degrade norfloxacin by H_2O_2 at a wide initial pH. Besides, the degradation efficiency of acidic to neutral is better than that of strong alkaline[28]. Furthermore, many applications of iron-related hydrogen peroxide degraded pollutants are biased towards neutral pH[29,30]. Nie et al. demonstrated that acid red B (ARB) degradation efficiency by H_2O_2 is best at neutral pH and the degradation rate increased with the decrease of initial pH value[29]. Jiang et al. proved that phenol degradation by H_2O_2 in initial neutral pH can achieve the best efficiency[30]. Nie et al. degrade dimethyl phthalate by H_2O_2 presents best at neutral pH[28]. Therefore, an anode material operating in a non-carbonate environment is very important.

However, there are only a few reports about 2e− WOR H_2O_2 generation in non-bicarbonate systems. Among them, Zinc (II) porphyrin, and Tin (IV)-porphyrins are water-soluble, and they need to adjust the sodium sulfate electrolyte to an alkaline environment to produce hydrogen peroxide[31,32]. Moreover, the H_2O_2 yield can only reach the nmo h^{-1} level. Although both C, N-doped TiO_2 and commercial fluorine-doped SnO_2 FTO glass can produce hydrogen peroxide via 2e− WOR in acidic sodium sulfate electrolyte, the hydrogen peroxide production rate is only 0.2900 $\mu M\,h^{-1}$ and 2.2794 $\mu mol\,h^{-1}$, respectively[33,34]. There are also cases where Na_2HPO_4 and NaH_2PO_4 are used as electrolytes in the field of water oxidation. These solutions are alkaline, while both the hydrogen peroxide yields are very low, 2.0589 and 1.3971 $\mu mol\,h^{-1}$, respectively[34]. It can be seen that the H_2O_2 yield is very low when there is no carbonate mediated for water oxidation to H_2O_2.

Li et al. present that H_2O_2 generation through both direct (via OH^-) and indirect (via HCO_3^-) pathways. *HCO_3 will be converted to *HCO_4 and the O-O bond form. It proves that percarbonate is the critical species generated through the conversion of bicarbonate at Ga-Ga dual sites because percarbonate will decompose to generate H_2O_2 and carbonate. Therefore, percarbonate is the crucial intermediate for the generation of H_2O_2. The peroxyl bond is stable on the surface of the $ZnGa_2O_4$ anode. This work demonstrates that the key point for the H_2O_2 generation is the formation of a crucial intermediate that stabilizes the O-O bond on the surface of the catalyst and the generation of H_2O_2 is affected by the stability of the crucial intermediate and the oxygen bond on the anode surface[22]. The presence of oxygen acid like carbonate is important in the process of water oxidation to produce hydrogen peroxide.

Actually, in the presence of carbonate, O-O is formed by the participation of carbonate in the solution and OH part in the water. Therefore, this inspires us that if OH and oxygen-acid can be provided, we can prepare H_2O_2 by a two-electron water oxidation strategy even without carbonate. If we want to increase the yield of hydrogen peroxide in the system without carbonate, the most important step is the formation of sufficient O-O bonds.

Sulfate is a very comment oxygen acid and it will be applicable if we can use sulfate to replace carbonate. However, compared to sulfate is difficult to react with OH from electrolytes to form O-O bond. In our opinion, to achieve this, a suitable catalyst is required to work, which can provide OH to contribute to the reaction.

Herein, we achieve this goal by using basic copper carbonate ($Cu_2(OH)_2CO_3$), which is commonly found on the surface of copper. We discover that these materials contain lattice OH in its structure, and we achieve the production of H_2O_2 via the 2e− WOR method in non-carbonate Na_2SO_4 electrolyte on a tablet basic copper carbonate independent anode. A crystal OH mediating pathway for the generation of hydrogen peroxide in non-carbonate Na_2SO_4 electrolyte. SO_4 in the electrolyte combined with the crystal OH part in $Cu_2(OH)_2CO_3$ to form SO_4OH^*. SO_4OH^* is further transferred to OOH and SO_3. The O-O the band is formed. This O-O bond length is calculated to be 1.47 Å by DFT, which is close to the O-O bond length of 1.48 Å in H_2O_2. The combination of OOH and H from H_2O would form H_2O_2. Meanwhile, the remaining OH in water combines with $Cu_2(OH)CO_3$ and returns to $Cu_2(OH)_2CO_3$. SO_3 combined with another H_2O to form $SO_3·H_2O$. SO_3 part in $SO_3·H_2O$ combines with OH in water to form HSO_4^* and release a H^+. And then the HSO_4^* ionizes to produce a SO_4^{2-} and another H^+. This pathway provides an idea in the field of hydrogen peroxide production. It provides a method for hydrogen peroxide production via two-electron water oxidation in a non-carbonate system.

Results

H_2O_2 electro-synthesis via 2e− water oxidation in Na_2SO_4 electrolyte by $Cu_2(OH)_2CO_3$ tablet

The production of H_2O_2 in a non-carbonate electrolyte is a challenging task. For instance, when graphite is used as the anode in a non-carbonate electrolyte of Na_2SO_4, it cannot oxidize water to generate H_2O_2. In contrast, loading basic copper carbonate powder onto carbon paper (Fig. 1a) as the anode can produce 26.32 μM of hydrogen peroxide in 120 min under 3.4 V vs. RHE, which is much better than the widely-used graphite anode. However, the loaded powder of basic copper carbonate quickly falls off from the carbon paper (see Text S12 for more details), the comparison as illustrated in Fig. 1a, leading to a stagnant H_2O_2 concentration in the later stage. To address this issue, the catalyst is directly pressed into a solid tablet as the anode, as shown in Fig. 1b. In our experiment, it is observed that $Cu_2(OH)_2CO_3$ powder can be pressed into a tablet block (Fig. 1b) with the addition of a 60% PTFE binder. It's due to that the $Cu_2(OH)_2CO_3$ powder could not be pressed into a tablet block without PTFE preprocessing regardless of the applied pressure (details shown in Text S4 of the supplementary information). The $Cu_2(OH)_2CO_3$ tablet before and after use showed no significant variation, as depicted in Fig. 1b. This comparison diagram indicates that the basic copper carbonate tablet block electrode is superior to loading the powder on carbon paper. Additional, physical properties of $Cu_2(OH)_2CO_3$ are shown in Text S13. When the $Cu_2(OH)_2CO_3$ tablet is used directly as the anode, the hydrogen peroxide yield (1065.16 μM) under a potential of 3.4 V vs. RHE is significantly improved compared to loading on carbon paper (26.32 μM), as shown in Fig. 1c, with a 40-fold improvement. It is confirmed that the product is indeed hydrogen peroxide, as discussed in Text S6 and Text S7 of the supplementary information.

Furthermore, the H_2O_2 yield under different potentials using a basic copper carbonate tablet anode in a 50 mL 0.5 M Na_2SO_4 electrolyte solution is shown in Fig. 1d. The hydrogen peroxide yield

concentration increases with the voltage increase due to the increase in current (Fig. S1). However, when the potential rises to 3.6 V vs. RHE, the hydrogen peroxide yield concentration decreases because the excessive voltage may decompose a large amount of the generated hydrogen peroxide and oxygen evolution. The highest hydrogen peroxide yield concentration is achieved at 3.4 V vs. RHE (1065.16 μM) in the voltage range of 1.8–3.6 V vs. RHE. The corresponding hydrogen peroxide generation rate under different potentials are shown in Fig. 1e. The generation rate at 3.4 V vs. RHE high to 64.35 μmol h^{-1}, and Faradaic efficiency high to 66.76% at 1.8 V vs. RHE. These results are higher than existing reports related to non-carbonate researches (as listed in Table S1). Additionally, experimental results from 16 cycles of 8-hour operation have demonstrated the stability of the performance of Cu$_2$(OH)$_2$CO$_3$ tablet. It is illustrated in Fig. 1f. The current values monitoring in 8 h are stabilized at 20 ~ 22 mA. The FE values are basically stable between 20 ~ 30%. It reflects that the Cu$_2$(OH)$_2$CO$_3$ tablet can be stable in Na$_2$SO$_4$ electrolyte in water oxidation reaction to hydrogen peroxide product process.

Furthermore, we also investigated the performance of Cu$_2$(OH)$_2$CO$_3$ tablet electrodes for water oxidation to produce hydrogen peroxide in other electrolyte solutions without carbonate, such as NaNO$_3$, Na$_2$SiO$_3$, and NaAc solutions. The results are depicted in Fig. S11 and Fig. S12. It indicates that Cu$_2$(OH)$_2$CO$_3$ tablet electrode can approach the production of hydrogen peroxide through water oxidation in both NaAc and NaNO$_3$ solutions. By comparing the current in these four non-carbonate salt electrolyte solutions and the pH

values listed in Table S6, it can be observed that our Cu$_2$(OH)$_2$CO$_3$ tablet electrode is more suitable for operation in neutral electrolytes.

Characterization of Cu$_2$(OH)$_2$CO$_3$ tablet

The morphology of the Cu$_2$(OH)$_2$CO$_3$ tablet is characterized by the SEM images, as shown in Fig. 2a. The filaments in all images originate from the PTFE binder, which acts to better bond the basic copper carbonate microspheres together so that they can be pressed into a tablet solid. There is no significant change in the size of the microspheres before and after the reaction, and they are all about 250 nm. The overall morphology and arrangement of the microspheres do not change significantly before and after the reaction. Figure 2b shows the comparison of FTIR spectra of Cu$_2$(OH)$_2$CO$_3$ tablets before and after use. The emerging band at 1379, 558, 497, 428 cm^{-1} are assigned to SO$_3$·H$_2$O[35–39]. The emerging bands at 1090 and 506 cm^{-1} correspond to γ_3-SO$_4^{2-}$ vibration which originates from the residual SO$_4^{2-}$ from aqueous electrolyte[40,41]. The band at 1205 cm^{-1} is owing to the antisymmetric stretching vibration of CF$_2$, which is from the addition of PTFE binder in tablet anode[42–44]. The band at around 1150 cm^{-1} is attributed to the superposition of symmetric stretching vibration of CF$_2$ and γ_3-SO$_4^{2-}$ from residual Na$_2$SO$_4$ crystal[40,42,43]. The crystallinity of the tablet is characterized by XRD which shown in Fig. 2c, the tablet before and after reaction show typical 2θ peaks at 14.8°, 17.6°, 24.1°, 31.2° and 35.6°, which are assigned to the (0 2 0), (1 2 0), (2 2 0), (2 0 -1), (2 4 0) planes of Cu$_2$(OH)$_2$CO$_3$ (PDF#41-1390). It proves that the composition in the pressed solid anode is indeed basic copper carbonate. Fig. 3.
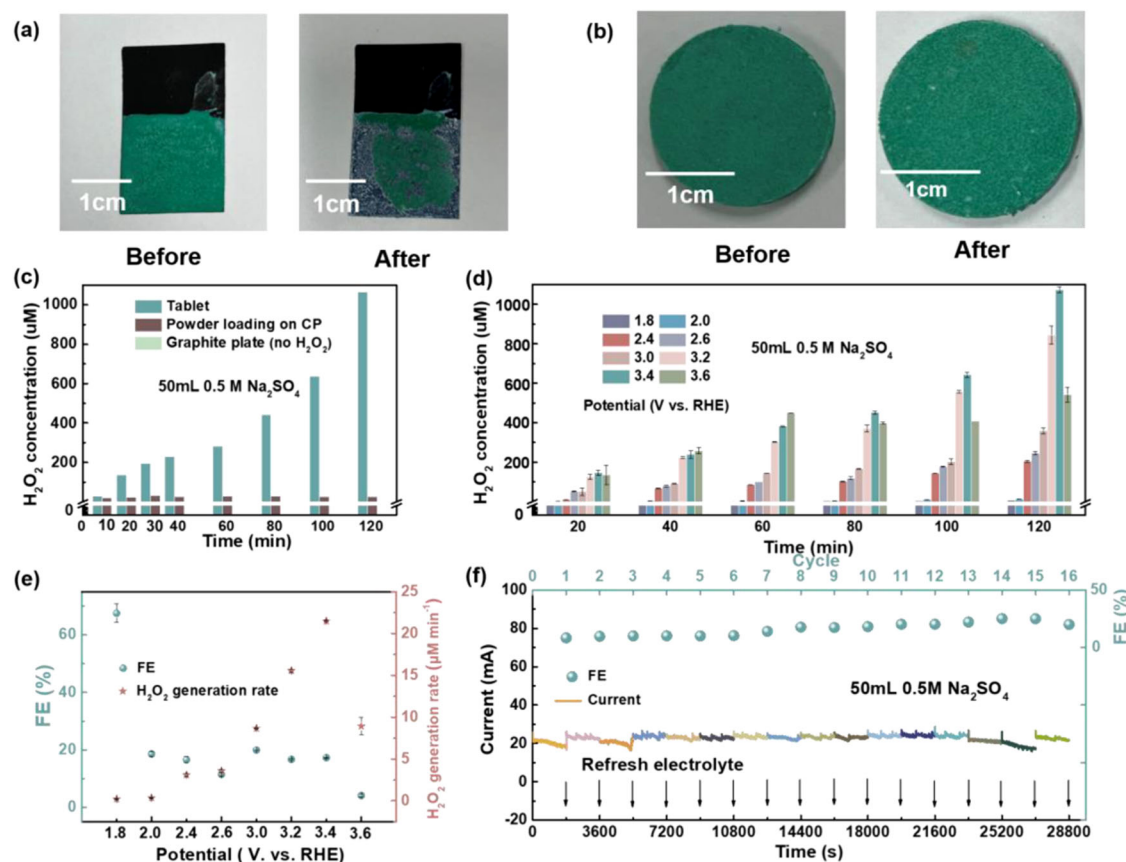
Fig. 1 | Performance of Cu$_2$(OH)$_2$CO$_3$ tablet electrode in H$_2$O$_2$ production by water oxidation pathway. a Comparison of Cu$_2$(OH)$_2$CO$_3$ powder loading on carbon paper as electrode before (left) and after (right) reaction. **b** Cu$_2$(OH)$_2$CO$_3$ tablet as electrode before (left) and after (right) reaction. **c** H$_2$O$_2$ yield in 50 mL 0.5 M Na$_2$SO$_4$ electrolyte at 3.4 V vs. RHE. **d** H$_2$O$_2$ yield in 50 mL 0.5 M Na$_2$SO$_4$ electrolyte under different potential. **e** H$_2$O$_2$ generation rate and faradic efficiency of Cu$_2$(OH)$_2$CO$_3$ tablet under different potential. **f** I-t curves and FE at 30 min in 8 h of Cu$_2$(OH)$_2$CO$_3$ tablet in 50 mL Na$_2$SO$_4$ electrolyte by refreshing electrolyte per 30 min (16 cycles). Error bars represent the standard deviation of three measurements. Source data for Fig. 1c–f are provided as a Source Data file. The voltage is not iR corrected in all electro-experiments. The mass of the active materials in all comparative experiments is 2 g.
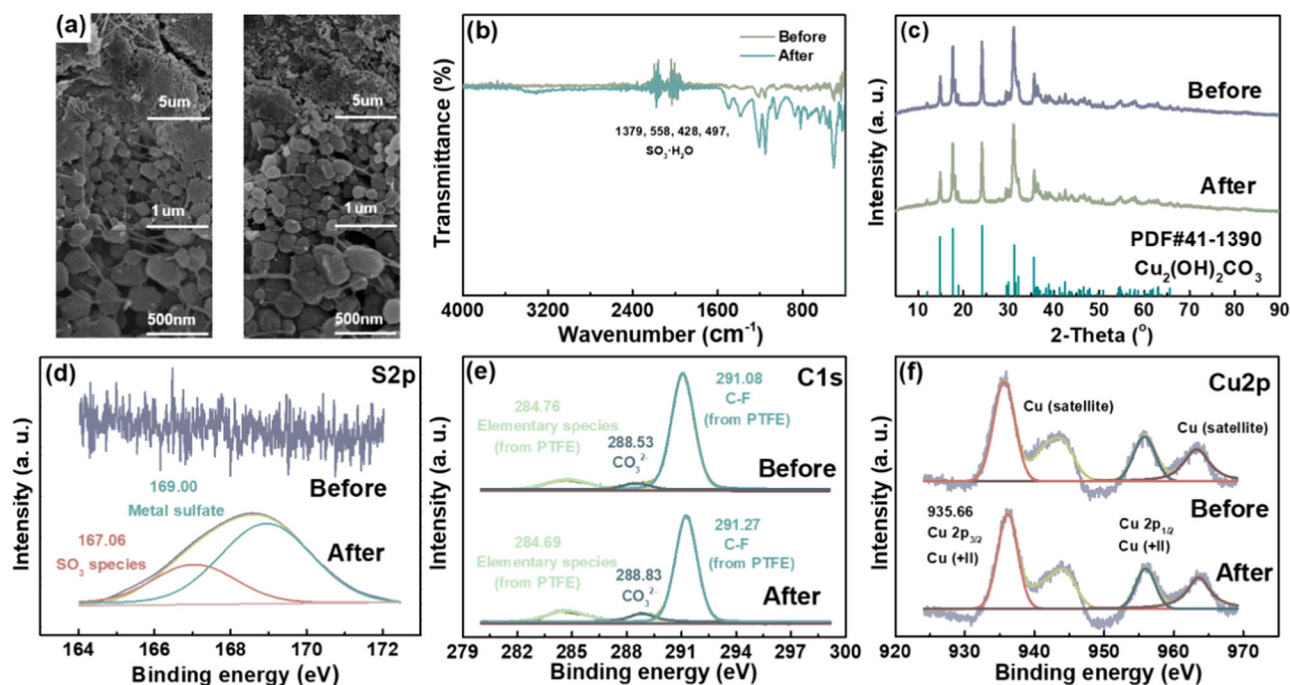
Fig. 2 | Characterization of Cu₂(OH)₂CO₃ tablet. a SEM images of Cu₂(OH)₂CO₃ tablets before (left) and after (right) reaction. **b** Fourier infrared absorption spectra (FTIR) of Cu₂(OH)₂CO₃ tablets before and after reaction in the wave number range of 400–4000 cm⁻¹. **c** XRD patterns of Cu₂(OH)₂CO₃ tablets in the 2-theta range of 5–90°. **d** S 2*p* high-resolution XPS survey spectra of Cu₂(OH)₂CO₃ tablets before and after reaction. **e** C 1*s* high-resolution XPS survey spectra of Cu₂(OH)₂CO₃ tablets before and after reaction. **f** Cu 2*p* high-resolution XPS survey spectra of Cu₂(OH)₂CO₃ tablet before and after reaction. Source data for Fig. 2b–f are provided as a Source Data file.

Figure 2d–f are S 2*p*, C 1*s*, and Cu 2*p* high-resolution XPS survey spectra of Cu₂(OH)₂CO₃ tablets before and after reaction, respectively. Since there is no S element on the Cu₂(OH)₂CO₃ tablet anode before the reaction, the S 2*p* high-resolution XPS survey spectrum here only has the result after the reaction (Fig. 2d). The S 2*p* spectrum is fitted into two peaks at the binding energy of 167 eV and 169 eV, which are corresponding to SO₃ species and metal sulfate[45,46]. The existence of SO₃ species corresponds to the occurrence of SO₃ after the reaction shown in Fig. 2b, which confirms the existence of SO₃ · H₂O residue after the reaction. The emergence of metal sulfate is due to the residual electrolyte sodium sulfate. The C 1*s* spectra are fitted into three peaks with the binding energies of 284.5, 288.5, and 291 eV as shown in Fig. 2e, which can be assigned to elementary species, CO₃²⁻ carbon species, and C-F₂, respectively[47–50]. Among them, elementary species refers to the skeleton carbon such as CH₂, which and C-F₂ are derived from the binder PTFE in the tablet. CO₃²⁻ is origin from basic copper carbonate. Carbon in PTFE accounts for a large proportion of the overall C 1*s* spectra because PTFE is an organic substance, which contains a large amount of carbon. While basic copper carbonate is an inorganic substance, so the proportion of carbon is relatively small. The C 1*s* spectra before and after the reaction present similar results. In the Cu 2*p* spectra as depicted in Fig. 2f, Cu 2*p* normally spin-orbit couples into two peaks as well as several shake-up satellite peaks at 941 eV, 944 eV, and 963 eV. The binding energy of Cu 2*p*₃/₂ and Cu 2*p*₁/₂ at around 935 eV and 955 eV are addressed to copper ions Cu²⁺, which confirmed the existence of Cu₂(OH)₂CO₃[51–53]. There is no emerging peak after the reaction in the C 1*s* spectrum. The above characterization results show that the surface electronic states and the chemical elemental composition of the Cu₂(OH)₂CO₃ tablet are stable.

Electrochemical performance of Cu₂(OH)₂CO₃ tablet

LSV curves recorded in 0.5 M Na₂SO₄ at the scan rate of 50 mV s⁻¹ are shown in Fig. 3a. It shows that the current increases dramatically when

it exceeds 1.8 V vs. RHE. Figure 3b is the capacitance-potential (C-P) curves of Cu₂(OH)₂CO₃ tablet and graphite concluded by Chronopotentiometry measurement. It is used to determine the electrochemically active surface areas (EASA) of the Cu₂(OH)₂CO₃ tablet and graphite anode. Specifically, a constant current density of 1 mA was applied to the Cu₂(OH)₂CO₃ tablet with a potential window of 1.2 V, while the graphite anode was carried out with a constant current density of 0.5 mA in the potential windows of 0.4 V. The following equation can be used to estimate the specific capacitance C of Cu₂(OH)₂CO₃ tablet and graphite anode from the potential-time curves[54,55].

$$C = \frac{I^{*}\Delta t}{\Delta V} \tag{2}$$

Where I present the current density during Chronopotentiometry measurement processes, t presents the time, and ΔV presents the potential window.

During this measurement, I and ΔV are considered constants. After substituting the corresponding values into the above Eq. (2), the specific capacitance C of Cu₂(OH)₂CO₃ tablet and graphite can be calculated to be 16.67 and 50 mF, respectively. Usually, the electrochemically active surface areas can be calculated by using a ratio between capacitance and specific surface area. Taking a value of 14 μF cm⁻²[54], the electrochemical specific surface area of the Cu₂(OH)₂CO₃ tablet and graphite is 1189 and 3571 cm² per geometric cm², respectively. Although the electrochemically active surface areas of graphite are much larger than that of tablet basic copper carbonate. However, a relative experiment shows that graphite cannot produce hydrogen peroxide through water oxidation in Na₂SO₄ electrolyte solution. Therefore, even if graphite has large electrochemically active surface areas, there is no active site that can produce hydrogen peroxide in Na₂SO₄ solution. Figure 3c shows the Electrochemical impedance of Cu₂(OH)₂CO₃ tablet in Na₂SO₄ with different pH. The AC impedance is
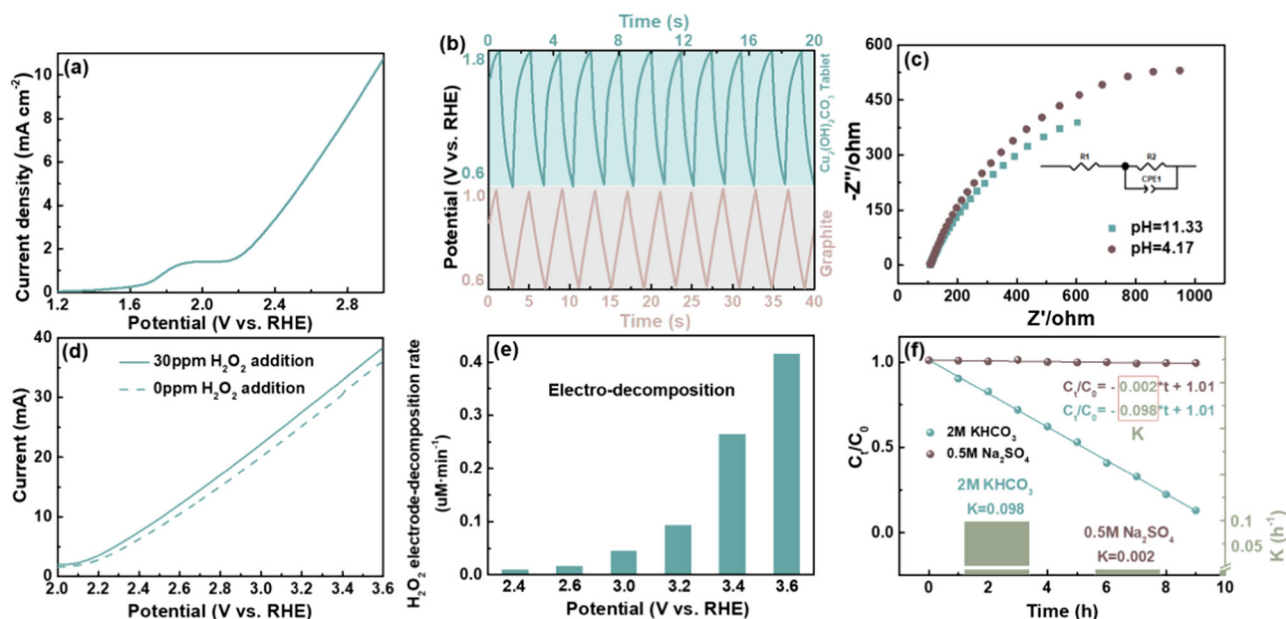
Fig. 3 | Electro-chemical performance of Cu₂(OH)₂CO₃ tablet. a LSV curves recorded in 2 M KHCO₃ at a scan rate of 50 mV s⁻¹ of Cu₂(OH)₂CO₃ tablet anode. **b** Galvanostatic charge/discharge behaviors of Cu₂(OH)₂CO₃ tablet and graphite oxide with an applied constant current density of 1 (Cu₂(OH)₂CO₃ tablet) and 0.5 (graphite) mA cm⁻² measured by Chronopotentiometry measurement. **c** Nyquist plots of Cu₂(OH)₂CO₃ tablet anode in 50 mL 0.5 M Na₂SO₄ with different pH and corresponding fitting circuit diagram. **d** LSV curves were recorded in 0.5 M Na₂SO₄ electrolyte with or without 30 ppm H₂O₂ addition at a scan rate of 50 mV s⁻¹ of

Cu₂(OH)₂CO₃ tablet. **e** Electro-decomposition rate of H₂O₂ on Cu₂(OH)₂CO₃ tablet anode at different potentials in 0.5 M Na₂SO₄. **f** Self-decomposition rate constants of H₂O₂ with 1 mM initial concentrations in 2 M KHCO₃ or 0.5 M Na₂SO₄ solution. pH error bars represent the standard deviation of three measurements. Acidic (4.17 ± 0.1), basic (11.33 ± 0.07), and the initial pH of 0.5 M Na₂SO₄ (7.15 ± 0.15). Source data for Fig. 3a–f are provided as a Source Data file. The voltage is not iR corrected in all electro-experiments.

smaller in an environment with a pH of 11.33 than in an environment with a pH of 4.17, which may be because there are more mobile ions in the environment of 11.33. The AC impedance was fitted with the analog circuit illustrated in Fig. 3c. The fitted solution resistance (R1) and charge transfer resistances (R2) in the Nyquist plot were 1258 ± 10 Ω (11.33) and 14978 ± 38 Ω (4.17), respectively.

Besides, the decomposition of H₂O₂ on the electrode surface is investigated by the following experiments according to related references [56,57]. Specifically, the LSV curves of the basic copper carbonate tablet anode were scanned in the Na₂SO₄ electrolyte solution with or without 30 ppm H₂O₂ addition, and the obtained results are shown in Fig. 3d. The I-V curve exhibits a negative shift when with 30 ppm H₂O₂ addition compared with the curve obtained without H₂O₂ addition. It is due to the anodic oxidation decomposition of hydrogen peroxide on the electrode surface. Figure 3e is the electro-decomposition rate of H₂O₂ on Cu₂(OH)₂CO₃ tablet anode at different potentials. This calculation refers to the method in the relevant literature[58] (see Text S8 of supplement information). It shows that the electro-decomposition rate on Cu₂(OH)₂CO₃ tablet anode increases with the increase of voltage. This is why the concentration of H₂O₂ decreases when the voltage is too high. The difference in the production of hydrogen peroxide in the carbonate-free electrolyte system comes from the difference in the active site, which is not found in graphite.

Besides, Na₂SO₄ solution as an electrolyte is still superior to KHCO₃ because the self-decomposition ratio in Na₂SO₄ is much smaller than in KHCO₃. The experimental details are shown in Text S5. The results shown in Fig. 3f indicates that the decomposition rate constants are determined to be 0.098 h⁻¹ in KHCO₃, which is indeed smaller than 0.002 h⁻¹ in Na₂SO₄. Subsequently, to further explore the mechanism of tablet basic copper carbonate producing hydrogen peroxide in Na₂SO₄ solution, the following series of experiments are carried.

Influence of carbonate in the liquid phase

To determine whether the H₂O₂ produced by Cu₂(OH)₂CO₃ tablet is derived from the effect of carbonate dissolved in the solution, a control experiment is conducted. 2 g Cu₂(OH)₂CO₃ powder and the Cu₂(OH)₂CO₃ tablet are put into two separate 50 mL 0.5 M Na₂SO₄ solutions. These two solutions remain colorless after 2 h, as shown in Fig. 4a. Solid basic copper carbonate powder is visible in the aqueous phase. Copper ions in aqueous solutions typically appear green, but no green color is observed in this experiment. Additionally, UV-vis adsorption of solutions at different times showed no peaks, and the entire curve was almost horizontal (Fig. S3). By contrast, the UV spectra of the Cu²⁺ solution in Fig. S4 show obvious peaks in the same wavelength scanning range, indicating that Cu²⁺ is present in the solution. These results suggest that basic copper carbonate is not dissolved in a neutral Na₂SO₄ solution.

Furthermore, another control experiment is conducted using a graphite plate as the anode and 2 g basic copper carbonate powder directly dispersed into the 50 mL 0.5 M Na₂SO₄ electrolyte solution in the anode cell under the same potential of 3.4 V vs. RHE. It is known that graphite can oxidize water to produce H₂O₂ in an electrolyte system with carbonate, which reached 832 μM under the potential of 3.4 V vs. RHE at 120 min in 50 mL KHCO₃ as shown in Fig. 4b. However, the results showed that no H₂O₂ was produced in this Na₂SO₄ and basic copper carbonate powder mixture electrolyte (Fig. 4b). It indicates that basic copper carbonate and sodium sulfate solution cannot produce carbonate that has an effectual effect in the water oxidation process to produce hydrogen peroxide. In summary, it is confirmed that the production of H₂O₂ in a Na₂SO₄ electrolyte solution by a Cu₂(OH)₂CO₃ tablet is not derived from carbonate in the solution.

Experiments are conducted using a basic copper carbonate tablet as an anode in different concentrations of Na₂SO₄ at 3.4 V vs. RHE. The results shown in Fig. 4c indicate that the hydrogen peroxide yield increases with an increase in the concentration of Na₂SO₄ electrolyte. It
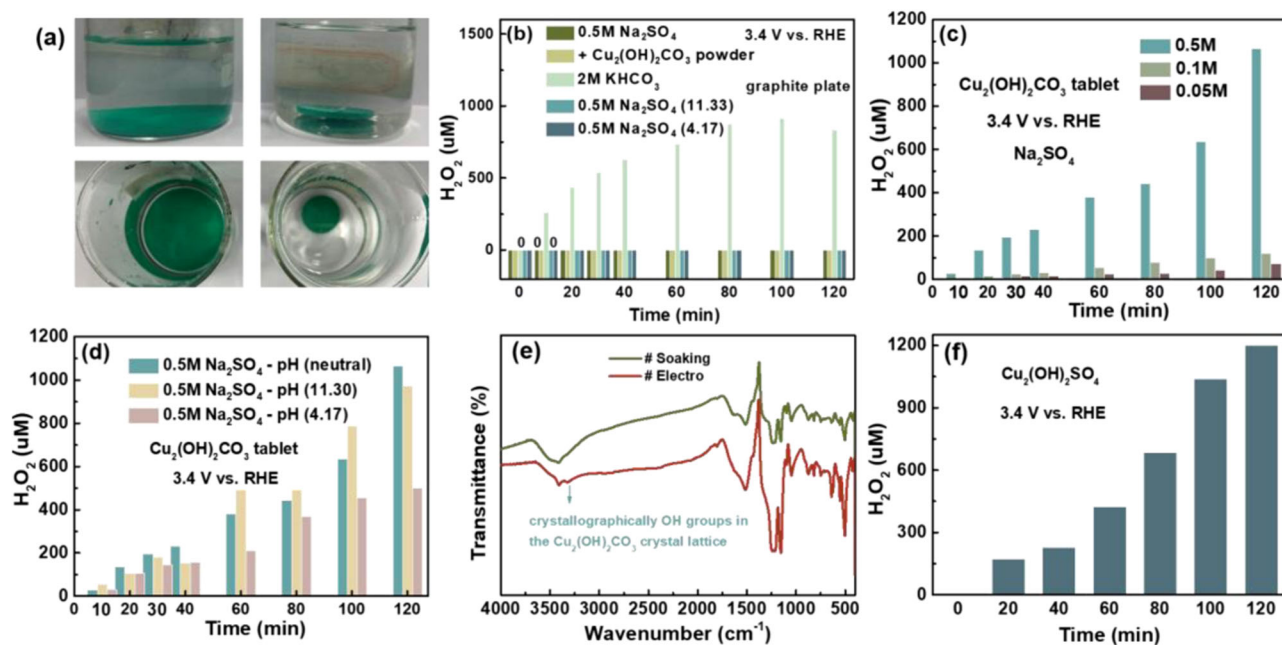
Fig. 4 | Investigation of the active component of the Cu₂(OH)₂CO₃ tablet Electrode. **a** Picture of 50 mL 0.5 M Na₂SO₄ solution with Cu₂(OH)₂CO₃ tablet or Cu₂(OH)₂CO₃ powder addition. **b** H₂O₂ production concentration of graphite under the potential of 3.4 V vs. RHE in different electrolyte. **c** H₂O₂ concentration of Cu₂(OH)₂CO₃ tablet in different concentration of Na₂SO₄ electrolyte under the potential of 3.4 V vs. RHE. **d** H₂O₂ concentration of Cu₂(OH)₂CO₃ tablet in Na₂SO₄ solution with different pH under the potential of 3.4 V vs. RHE. **e** FTIR spectra of Cu₂(OH)₂CO₃ obtained from Isotope O¹⁸ tracing experiments. **f** H₂O₂ generation properties of Cu₂(OH)₂SO₄ tablet in 50 mL Na₂SO₄ under 3.4 V vs. RHE. The results in Fig. 4b–f are all obtained from a 50 mL electrolyte system. Source data for Fig. 4b–f are provided as a Source Data file. The voltage is not iR corrected in all electro-experiments. The mass of the active materials in all comparative experiments is 2 g.

suggests that sulfate in electrolyte may play a role in the production of hydrogen peroxide in the system, and a higher concentration of sulfate is more conducive to the production of hydrogen peroxide.

Another difference between Na₂SO₄ and KHCO₃ solutions is the pH of the solution. An alkaline electrolyte is known to be conducive to water oxidation to produce hydrogen peroxide. To investigate the effect of pH of the electrolyte on the electro-synthesis of the hydrogen peroxide process on the basic copper carbonate tablet, experiments were designed. The pH of the 0.5 M Na₂SO₄ solution in the anode cell was adjusted to 11.33 by NaOH, but no hydrogen peroxide production was observed in this non-carbonate basic electrolyte by graphite anode, as shown in Fig. 4b. It indicates that for graphite anodes, only an alkaline environment is not enough, and the presence of carbonates is necessary to water oxidation to produce hydrogen peroxide. By contrast, the basic copper carbonate tablet can produce hydrogen peroxide in a system without carbonate in a neutral Na₂SO₄ electrolyte.

The effect of the pH of the electrolyte solution on the production of hydrogen peroxide on a Cu₂(OH)₂CO₃ tablet is investigated (Fig. 4d). At pH = 11.33, the yield of hydrogen peroxide is almost the same as that when the pH is not adjusted. At pH = 4.17 by H₂SO₄, the basic copper carbonate sheet could still produce hydrogen peroxide in an acidic electrolyte, although the yield of hydrogen peroxide is reduced by half to 501 μM at 120 min. The basic copper carbonate tablet can produce H₂O₂ in a solution without carbonate, but the acidic environment makes the production of H₂O₂ less than that of neutral or alkaline, which is consistent with previous literature conclusions[56,57]. Because the 2e⁻ WOR water oxidation process will release H⁺ (Eq. (3)). The presence of excessive products can hinder the forward progress of the reaction. Therefore, Eq. (3) can reflect that the presence of excessive H⁺ is unfavorable for the formation of hydrogen peroxide. Moreover, the results of Nyquist plots show that the AC impedance of the Cu₂(OH)₂CO₃ tablet anode in the acidic electrolyte is larger than that in the alkaline electrolyte. It suggests that alkaline electrolytes can

neutralize the generated H⁺ from water oxidation[21], which is beneficial to the forward progress of the reaction. If it is an acidic electrolyte, the generated H⁺ accumulates continuously, which is not conducive to the forward progress of the reaction. From this perspective, it will be more difficult to produce hydrogen peroxide by water oxidation in an acidic electrolyte.

$$2H_2O \rightarrow H_2O_2 + 2H^+ + 2e^- \tag{3}$$
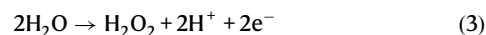
Furthermore, graphite as the anode could not produce hydrogen peroxide in Na₂SO₄ solutions at any pH, as shown in Fig. 4b and Table S5. It could only produce H₂O₂ in KHCO₃ solution. It indicates that the difference in the production of hydrogen peroxide in the carbonate-free electrolyte system comes from the difference in the active site, which is not found in graphite.

Influence of composition in Cu₂(OH)₂CO₃ tablet solid anode

The role of the compositions of basic copper carbonate tablet block in the 2e⁻ WOR process to produce hydrogen peroxide is further investigated. The following experiments are conducted and the results are shown in Table S4. Firstly, to study the role of the carbonate structure in Cu₂(OH)₂CO₃ tablet solid anode, CaCO₃ was used as the anode for comparison. As the structure of CaCO₃ is similar to that of the copper carbonate in basic copper carbonate. This result shows that the CaCO₃ anode cannot catalyze water oxidation to produce H₂O₂, which indicates that the CO₃ part in the solid anode should not play a key role in the production of hydrogen peroxide in a non-carbonate electrolyte system. Subsequently, the role of Cu part is investigated. We utilize CuO as the anode in a comparative experiment. The result shows that CuO as an anode could not catalyze water oxidation to produce H₂O₂ either. It turns out that it may not be Cu part in Cu₂(OH)₂CO₃ that determines this process. However, the previous results showed that there is indeed an active part in the basic copper carbonate. Therefore,

Table 1 | O¹⁸ abundance results

	$^\delta O^{18}$ (‰)	Standard deviation
#Elecro	270.59	0.25
#Soaking	/	/

we believe that the OH part of the $Cu_2(OH)_2CO_3$ tablet plays a certain role in the H_2O_2 production by $2e^-$ water oxidation process.

Evidence of cyclic exchange between O in crystal OH and O in H_2O

To demonstrate the role of the crystal OH component, we have designed three sets of experiments with the following thematic approach:

Firstly, to demonstrate the exchange between the O in H_2O and the O within the crystal of $Cu_2(OH)_2CO_3$ (Isotope O^{18} tracing method). Results are shown in Table 1, the results indicate that after the electrochemical reaction in the O^{18} electrolyte, samples were thoroughly washed, and O^{18} was detected in the electrolyte after subsequent electrochemical reaction in the O^{18}-free electrolyte. This observation suggests the presence of O^{18} alternating between the $Cu_2(OH)_2CO_3$ tablet and the electrolyte solution. Furthermore, samples that were soaked for the same duration in the O^{18} electrolyte, followed by thorough washing and subsequent electrochemical reaction in the O^{18}-free electrolyte, did not exhibit the presence of O^{18} in the electrolyte. It eliminates the potential influence of adsorption effects during the experimental process. These results provide evidence that O^{18} has indeed entered the crystal of $Cu_2(OH)_2CO_3$. It is demonstrated that the O from the $Cu_2(OH)_2CO_3$ tablet electrode undergoes a cyclic exchange process with the O in H_2O.

Secondly, to prove that the exchanged O originates from the OH component within the crystal of $Cu_2(OH)_2CO_3$. GC-MS analysis confirms the absence of O^{18} in the CO_2 gas produced during high-temperature decomposition, while FTIR analysis demonstrates the presence of $O^{18}H$ in the crystal OH groups in $Cu_2(OH)_2CO_3$. The results are shown in Fig. 4e and Fig. S9 in Supporting information. Using PY-GCMS analysis, it was determined that there was no presence of O^{18} in the generated gas (Fig. S9). The gas produced during the high-temperature formation of $Cu_2(OH)_2CO_3$ contained CO_2, indicating that the oxygen in CO_2 did not contain O^{18}. The O^{18} in CO_2 originated from the CO_3 component within $Cu_2(OH)_2CO_3$, suggesting that the CO_3 component did not contain O^{18}. Combining this with experimental findings from isotope O^{18} tracing experiments, where O^{18} was found to enter the lattice of $Cu_2(OH)_2CO_3$, it can be inferred that the O^{18} is located in the O of the OH component within the lattice of $Cu_2(OH)_2CO_3$. For FTIR spectrum (Fig. 4e), specific chromophores in molecules exhibit unique absorption capabilities at different wavelengths. The absorption wavelength of a specific vibrational mode depends on the mass of its atoms, which can be altered by substituting atoms with isotopes of different masses[59]. O^{18} significantly alters the absorption wavelength of this isotope-edited vibrational mode, allowing for the examination and orientation of individual transition dipole moments, with a negative frequency shift[59–61]. The spectrum of $Cu_2(OH)_2CO_3$ displays characteristic peaks in the range of 2500–4000 cm^{-1}, which can be assigned to the single-bond OH groups in the $Cu_2(OH)_2CO_3$ crystal[62,63]. It is observed in the Fig. 4e that the absorption peak at 3316 cm^{-2} is not prominent in the spectrum of #Soaking sample, but is pronounced in the spectrum of #Electro sample at that position. Introduction of O^{18}, as indicated Fig. 1 in Reference[59], results in a negative shift of the peak, suggesting that this is a consequence of O^{18} entering the crystal OH portion.

Finally, to verifying experiments, a confirmatory experiment to show that if the OH component is active rather than the O within the CO_3 component, then under similar conditions, replacing CO_3 with

other components should exhibit similar hydrogen peroxide production performance. As shown in Fig. 4f, $Cu_2(OH)_2SO_4$ tablets as the anode can produce hydrogen peroxide in Na_2SO_4, consistent with our expected results. Furthermore, the hydrogen peroxide yield is nearly identical to that of $Cu_2(OH)_2CO_3$. It suggests that replacing the CO_3 component with SO_4 can also lead to hydrogen peroxide production when the results are similar, indicating that CO_3 is not a critical component in the hydrogen peroxide production process. In addition, DFT calculation reveals that the SO_4^* cannot form HSO_5 intermediates if removing the OH from the $Cu_2(OH)_2CO_3$ structure (Fig. S17a), while can observed in the presence of OH (Fig. S17b). Combining the results above, it can be concluded that the OH component within the crystal undergoes cyclic exchange with O in H_2O.

DFT calculation of the interaction between $Cu_2(OH)_2CO_3$ and the electrolyte

Since CuO and $CaCO_3$ cannot produce hydrogen peroxide in Na_2SO_4 electrolyte solution under the same conditions. Then, it is speculated that the OH part plays an important role in the water oxidation process. Therefore, density functional calculation is conducted to study the interaction between $Cu_2(OH)_2CO_3$ and the electrolyte. The electrolyte mainly consists of OH^- and SO_4^{2-} ions. We study the OH^- from the electrolyte. According to calculation by density functional theory, there are two cases for the adsorption of OH^* from the electrolyte on the substrate: one with the OH^* adsorbed on the Cu atoms (Fig. 5a), and the other with the OH^* adsorbed on the O atoms via hydrogen bond (Fig. 5b). The adsorption energy is calculated by the following Eq. (4):

$$E_{ad} = E_{tot} - E_{substrate} - E_{OH} \qquad (4)$$

where E_{ad} is the adsorption energy, E_{tot} is the total energy of the molecule on the substrate, $E_{substrate}$ is the energy of the substrate, and E_{OH} is the energy of the OH adsorbed. The E_{ad} for the above-mentioned two cases is -3.3 eV and -4.8 eV, respectively. The negative value suggests that these two cases are possible to occur.

According to previous reports, the change of Gibbs free energy of $^*OH$ (ΔG_{OH^*}) is a crucial parameter for H_2O_2 production. The optimized range for directing oxidation of OH is between 1.6 to 2.4 eV[19]. However, the ΔG_{OH^*} is calculated to be about 0.70 eV when OH^* is adsorbed on Cu, and 0.82 eV when OH^* is adsorbed on O. These two values are not in the optimum range of 1.6 to 2.4 eV, suggesting directing oxidation of OH should not be the pathway for the generation of H_2O_2.

In addition to OH^-, SO_4^{2-} ions are the dominating ions in the electrolyte. Therefore, we further investigate the interaction between SO_4^{2-} and the substrate. As shown in Fig. 5c, an SO_4^{2-} ion is put near the substrate. Then, after structure relaxation, the structure of the SO_4^{2-} total changes (Fig. 5d). It is clear that the four O atoms rearrange. Interestingly, two O atoms link with each other to form the O-O bond, which is a very important bond for the production of H_2O_2. Importantly, some O atoms from the SO_4^{2-} are bonded with the OH from the substrate $Cu_2(OH)_2CO_3$, suggesting there are interactions between the SO_4^{2-} and the $Cu_2(OH)_2CO_3$ (Supplementary Data 1). Importantly, the O-O bond distance is found to be about 1.47 Å, which is very close to the O-O bond distance of 1.48 Å in H_2O_2. Therefore, this rearrangement of the SO_4^{2-} should be a crucial step for the production of H_2O_2. Therefore, to conclude, the generation of H_2O_2 should not be a direct pathway via OH^* adsorption. Instead, it should be an indirect pathway via SO_4^{2-}.

Crystal OH mediating pathway for hydrogen peroxide production

The O^{18} isotope tracing series of experiments demonstrated that the O from the crystal OH in the $Cu_2(OH)_2CO_3$ tablet electrode undergoes a cyclic exchange process with the O in H_2O. DFT calculations indicate
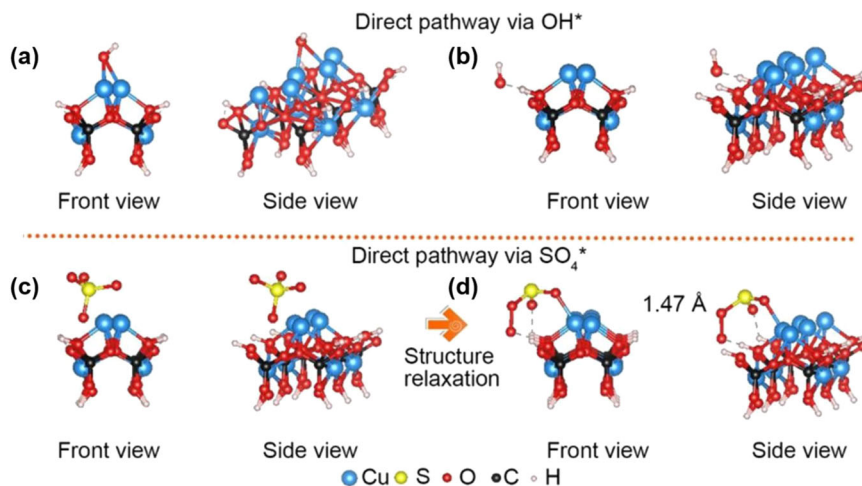
Fig. 5 | Direct pathway via OH* and indirect pathway via SO$_4$*. a Structure of OH* adsorbed on Cu atom and O atom on Cu$_2$(OH)$_2$CO$_3$ before structure relaxation. **b** Structure of OH* adsorbed on Cu atom and O atom on Cu$_2$(OH)$_2$CO$_3$ after structure relaxation. **c** Structure of SO$_4$* adsorbed on Cu$_2$(OH)$_2$CO$_3$ before structure relaxation. **d** Structure of SO$_4$* adsorbed on Cu$_2$(OH)$_2$CO$_3$ after structure relaxation.
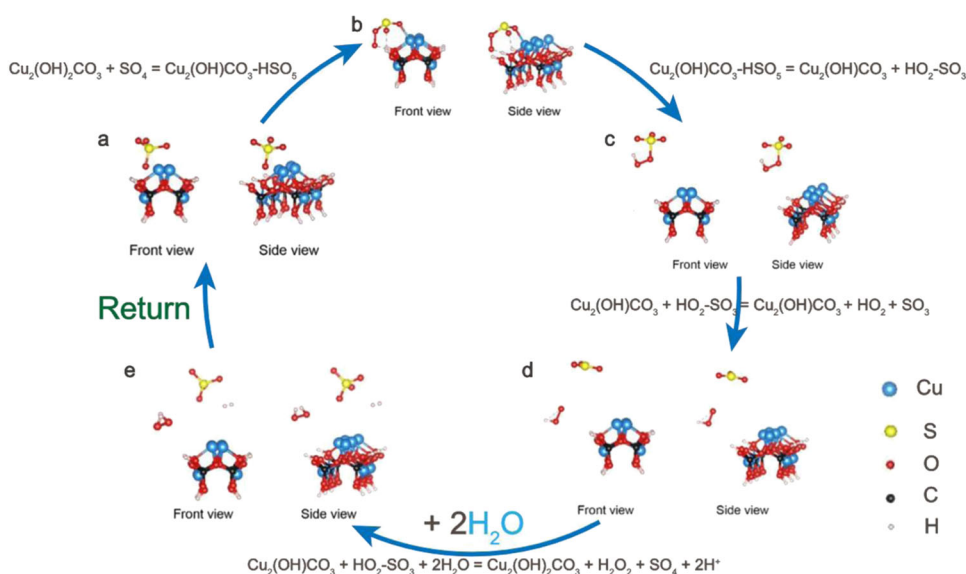
Fig. 6 | Diagram of H$_2$O$_2$ generation process on Cu$_2$(OH)$_2$CO$_3$. a Structural model of SO$_4$ on the surface of Cu$_2$(OH)$_2$CO$_3$. **b** SO$_4$ combines with OH in Cu$_2$(OH)$_2$CO$_3$ to form HSO$_5$. **c** HSO$_5$ structural reorganization forming HO$_2$-SO$_3$. **d** The bond in HO$_2$-SO$_3$ breaks, resulting in the formation of HO$_2$ and SO$_3$ intermediates. **e** HO$_2$ and SO$_3$ interact with two H$_2$O molecules to generate H$_2$O$_2$ while releasing two H$^+$, returning the SO$_4$ and Cu$_2$(OH)$_2$CO$_3$ original structure.

that this process occurs via an indirect pathway mediated by SO$_4^{2-}$ in the solution. To this end, we propose a crystal OH mediating pathway for hydrogen peroxide production via two-electron water oxidation. The crystal OH in the tablet electrode interacts with SO$_4$ in the electrolyte to form SO$_4$OH* intermediate. This intermediate subsequently decomposes into HO$_2$* and SO$_3$. The SO$_3$ intermediate contacts with H$_2$O, releasing two H$^+$ ions and SO$_4$ back into the solution. HO$_2$* combines with H from the H$_2$O to generate hydrogen peroxide, while the remaining OH returns to the crystal structure of the electrode, regenerating the Cu$_2$(OH)$_2$CO$_3$.

Figure 6 provides a detailed explanation of this process of H$_2$O$_2$ generation on Cu$_2$(OH)$_2$CO$_3$. Firstly, the SO$_4^{2-}$ is adsorbed near the OH of the Cu$_2$(OH)$_2$CO$_3$. The structure of the SO$_4^{2-}$ total change. It is clear that the four O atoms rearrange. Interestingly, two O atoms link with each other to form the O-O bond, which is a very important bond for the production of H$_2$O$_2$. The O-O bond distance is found to be about 1.47 Å, which is very close to the O-O bond distance of 1.48 Å in H$_2$O$_2$. This process is shown as Eq. (5) below. Therefore, this rearrangement

of the SO$_4^{2-}$ should be a crucial step for the production of H$_2$O$_2$.

$$Cu_2(OH)_2CO_3 + SO_4{}^{2-} = Cu_2(OH)CO_3 - HSO_5{}^{2-} \quad (5)$$

$$Cu_2(OH)CO_3 - HSO_5 = Cu_2(OH)CO_3 + HO_2 - SO_3 \quad (6)$$

$$Cu_2(OH)CO_3 + HO_2 - SO_3 = Cu_2(OH)CO_3 + HO_2 + SO_3 \quad (7)$$
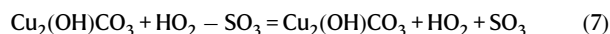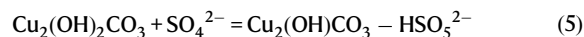
Subsequently, the HSO$_5$ part release from the Cu$_2$(OH)CO$_3$-HSO$_5$ and causes the following formation of HO$_2$ and SO$_3$ immediately. The process is demonstrated as Eqs. (6) and (7).

Then, two H$_2$O will take part in the reaction and produce H$_2$O$_2$, SO$_4^{2-}$ and 2H$^+$. In this step, one OH from H$_2$O will fill into Cu$_2$(OH)CO$_3$

and form $Cu_2(OH)_2CO_3$ again. The process is illustrated by Eq. (8).

$$Cu_2(OH)CO_3 + HO_2 + SO_3 + 2H_2O = Cu_2(OH)_2CO_3 + H_2O_2 + SO_4^{2-} + 2H^+ + 2e^-$$

(8)
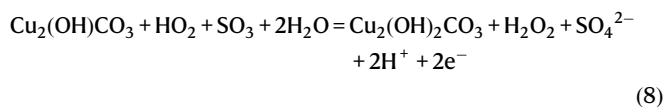
According to our calculation, the change of energy is about 2.625 eV. At the applied potential of 2.4 V vs. RHE, the change of energy is calculated to be about -2.17 eV, suggesting the reaction is thermodynamically favorable at this potential.

Therefore, to conclude, the generation of H_2O_2 should not be a direct pathway via OH* adsorption. Instead, it should be an indirect pathway via SO_4^{2-}, and the SO_4^{2-} and the OH from the $Cu_2(OH)_2CO_3$ contribute simultaneously to the formation of H_2O_2. The total reaction is expressed as Eq. (9):

$$Cu_2(OH)_2CO_3 + SO_4^{2-} + 2H_2O = Cu_2(OH)_2CO_3 + H_2O_2 + SO_4^{2-} + 2H^+ + 2e^-$$

(9)
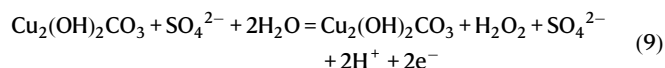
Discussion

In this study, the $Cu_2(OH)_2CO_3$ tablet anode is successfully prepared, which solved the problem that $Cu_2(OH)_2CO_3$ powder is easy to fall off during electrochemical experiments. More importantly, the use of $Cu_2(OH)_2CO_3$ tablet electrode successfully produced hydrogen peroxide by $2e^-$ water oxidation reaction in a carbonate-free electrolyte solution Na_2SO_4 solution, and the hydrogen peroxide production rate is as high as 64.35 µmol h^{-1}, and the Faradaic efficiency is up to 66.76%. Both the yield and Faradaic efficiency are higher than other the literature in non-carbonate electrolyte field. In addition, this study also verifies that the OH part in $Cu_2(OH)_2CO_3$ and sulfate radicals in electrolytes play key roles in the production of hydrogen peroxide through a series of comparative experiments. It's concluded that SO_4^{2-} attaches near the OH groups of $Cu_2(OH)_2CO_3$, causing a significant rearrangement of its structure and the $Cu_2(OH)CO_3 \cdot HSO_5$ is formed. Moreover, the release of HSO_5^- from $Cu_2(OH)CO_3 \cdot HSO_5$ prompts the formation of HO_2 and SO_3. O-O bond is crucial for H_2O_2 generation. The O-O bond distance of this HO_2 is approximately 1.47 Å, similar to that in H_2O_2. Subsequently, two H_2O molecules react, resulting in the production of H_2O_2, SO_4^{2-}, and $2H^+$. During this step, one OH from H_2O fills into $Cu_2(OH)CO_3$, return reforming $Cu_2(OH)_2CO_3$. This method enables hydrogen peroxide production in a neutral setting, expanding its environmental application potential. Although current density limitations exist, future research aims to enhance performance through anode modifications like nano-engineering and heterojunction construction. This study can inspire people to pay more attention to the contribution of lattice elements to the two-electron water oxidation reaction.

Methods

Chemicals

$Cu_2(OH)_2CO_3$ powder $Cu_2(OH)_2CO_3$, $KHCO_3$, $CaCO_3$, KCl, $Cu_2(OH)_2SO_4$ and DPD (N, N-diethyl-p-phenylene amine) are procured from Macklin Chemical Co. Na_2SO_4, Na_2HPO_4, NaH_2PO_4, and NaOH are purchased from Aladdin Chemical Co., Ltd. POD (horseradish peroxidase) with an enzyme activity of ≥ 300 U mg^{-1} is obtained from Sigma-Aldrich, Germany and stored in a dark environment at −2–8 °C. A 60% PTFE solution (Polytetrafluoroethylene) was purchased from Shanghai D&B Biological Science and Technology Co., Ltd. H_2SO_4 was procured from Merck, Germany, and copper oxide was purchased from Hebei Badu Metal Materials Co., Ltd. H_2O^{18} was purchased from Energy Chemical Co., Ltd. All chemicals are analytical grade and used without further purification, and ultrapure water is utilized in all experiments. The graphite plate is obtained commercially.

Preparation of $Cu_2(OH)_2CO_3$ tablet

A slurry was prepared by mixing 4 g of $Cu_2(OH)_2CO_3$ and 1 mL of 60% PTFE, which was then dried in an oven at 70 °C for 12 h to obtain PTFE-treated powder. 2 g of the dried powder was pressed into a $Cu_2(OH)_2CO_3$ pie-shaped tablet using a mold under a pressure of 10 kPa for 2 min, as depicted in Fig. 1b. For comparison, $Cu_2(OH)_2CO_3$ powder was loaded onto carbon paper by ultrasonically dispersing 2 g of the powder evenly in 1 mL 60% PTFE and 100 µL 0.1% Nafion mixture solution for 5 min, followed by drying in an oven at 70 °C for 12 h to form the anode as depicted in Fig. 1a. Additionally, when attempting to press the basic copper carbonate powder that was not treated with PTFE into a pie-shaped tablet using the same conditions, it remained in a powder state and could not be formed into a tablet. The electrode is depicted as a circular pie-shaped tablet with a radius of 1 cm. Please see Text S14 in Supporting Information for more details.

Characterizations

H_2O_2 was quantified by the DPD-POD method[19]. Specifically, a 0.3 mL sample was added into a 1.7 mL buffer. After 50 µL of DPD and POD addition, the mixture was scanned for UV curve and the absorption peak at 551 nm was used as a sign of H_2O_2 quantification. The morphology of samples was characterized by scanning electron microscope conducted by a QUANTAN FEG250 scanning electron microscope (SEM) at the accelerating voltages of 15–20 kV. The attenuated total reflection Fourier transform infrared (ATR-FTIR) spectra were collected in the ATR-FTIR mode using a Multimode In-Situ Infrared Spectrometer (Nicolet iS50) which was equipped with Golden Gate ATR attachment with diamond crystal and OMNIC software in the range of 400–4000 cm^{-1}. The X-ray diffraction (XRD) patterns were examined by using an UltimaIV X-ray diffractometer (Japan) with Cu Kα irradiation scan within 2-theta 5-90° to determine the crystal structure of the anode tablet. The X-ray photoelectron spectroscopy (XPS) was performed on a Thermo ESCALAB 250XI multifunctional imaging electron spectrometer (American Thermal Power, USA) to determine the surface electronic states and the chemical elemental composition of the $Cu_2(OH)_2CO_3$ tablets before and after the reaction. The instrument model of the stable water isotope analyzer is Picarro2140-i.

Electrochemical measurement

Preparation of Na_2SO_4 electrolyte solution. 71.021 g of Na_2SO_4 powder was dissolved in ultrapure water using magnetic stirring until fully dissolved. Then it was transferred to a 1 L volumetric flask and dilute to a final volume of 1 L. This solution is a 0.5 M Na_2SO_4 solution. The prepared electrolyte solution should be stored at room temperature in the dark as a reserve solution. Normally, if it is used within three days, a fresh solution will be prepared. If it is not used within three days, a fresh solution will be re-prepared.

Electrochemical measurement. The brand of the quartz electrochemical cell is Gaoshiruilian. The brand of the reference electrode is Chenhua. Specifically, the electrochemical system setup involved an H-type quartz electrolysis cell separated by Nafion 117 membranes (DuPond Co., the radius is 1.5 cm and the thickness is 183 µm, and it is sandwiched between two rubber rings and secured in the middle of two quartz electrolysis cells.), with 50 mL of 0.5 M Na_2SO_4 solution on each side serving as the electrolyte. The electrochemical setup consisted of a three-electrode system, with a carbon electrode as the counter electrode, an Ag/AgCl electrode (saturated potassium chloride solution) as the reference electrode and $Cu_2(OH)_2CO_3$ tablets as the working electrode. The experiments were conducted using a CHI 760E electrochemical workstation (Shanghai Chenhua Instrument Co., Ltd.). All tests were conducted at an ambient temperature of 25 °C. Potentials set against Ag/AgCl were converted to the RHE scale according to $E_{RHE} = E_{Ag/AgCl} + 0.197 + 0.059 \times pH$, and the pH values of electrolytes value were tested by a pH meter (Shanghai LeiMag Co.,

Ltd.). A graphite rod and a Ag/AgCl electrode (in a Luggin capillary) were used as the counter, and reference electrode, respectively. Cyclic voltammetry (CV) tests were carried out in this system at a scan rate of $50\,mV\,s^{-1}$. The charging/discharging behavior of the electrode is measured through chronopotentiometry. The Nyquist plot of the electrode is conducted by using the A.C. Impedance mode on the software connected to the electrochemical workstation.

Reference electrode calibration. In a $0.5\,M\,H_2SO_5$ electrolyte solution saturated with H_2, a Pt foil serves as the working electrode, while a carbon rod acts as the counter electrode, with an Ag/AgCl reference electrode immersed in saturated KCl solution. The scan rate is set at $50\,mV\,s^{-1}$, and the onset potential for hydrogen evolution obtained from the monitored hydrogen evolution curve is considered the zero potential relative to the RHE.

Faradaic efficiency calculation details. The Faradaic efficiency calculation details are shown below:

$$FE(\%) = \frac{m\,n\,96485}{Q}$$

Where, m represents the number of moles of produced hydrogen peroxide (mol), and n denotes the number of electrons transferred. This reaction is a two-electron process, thus n is a constant equal to 2. The value 96485 corresponds to Faraday's constant. Q represents the amount of charge transferred during the reaction, calculated as the product of time t (s) and current I (A).

Details of the isotope O^{18} tracing experiment. The aim of this experiment is to demonstrate that the oxygen in water indeed enters the crystal structure of $Cu_2(OH)_2CO_3$. Experimental Group: The $Cu_2(OH)_2CO_3$ pellets will operate at a voltage of 2.8 V vs. RHE in an electrolyte solution containing O^{18} for 2 h. After thorough washing, they will be placed in an electrolyte solution without O^{18} and operated at the same voltage for another 2 h. If the O^{18} from the electrolyte enters the $Cu_2(OH)_2CO_3$ crystal, it should be released back into the electrolyte upon further pressurization. The electrolyte solution obtained from the second electrochemical experiment will be collected and characterized using stable isotope analysis to determine the presence of O^{18}. Additionally, a control experiment will be conducted to eliminate any interference from adsorption effects. Control Group: The $Cu_2(OH)_2CO_3$ pellets will be soaked in an electrolyte solution containing O^{18} at room temperature for 2 h, followed by thorough washing. They will then be placed in an electrolyte solution without O-18 and operated at 2.8 V vs. RHE for 2 h. The electrolyte solution from the second operation will be analyzed for the presence of O^{18} isotopes.

Details for resistance measurements. The AC impedance fitting of sodium sulfate electrolyte solutions at different pH levels was performed. The R_s-(CPE-R_p) model from Instant Fit was selected, and the corresponding simulated circuit is illustrated in Fig. 3c for the fitting of the resistance parameters. The error bar is derived from the results of the cubic simulation.

Theoretical calculations. The mechanism for H_2O_2 generation is studied[19,64]. Projector-augmented-wave method with the Perdew–Burke–Ernzerhof of GGA functional was used[65–67]. The electronic convergence limit was set to be 1×10^{-5} eV[68]. Optimization of atomic coordinates was considered to be converged when the Hellmann–Feynman force was smaller than 1×10^{-2} eV $Å^{-1}$. The slab consisting of $Cu_2(OH)_2CO_3$ was established. Intermediate like SO_4^* are placed on the top of the surface. The vacuum region is about 15 Å in height. Detailed information is presented in Supplementary Data 1.

Data availability
Source data are provided with this paper. The data that support the findings of this study are available within the article and its Supplementary information files. Source data are provided with this paper.

References
1. Tanev, P. T., Chibwe, M. & Pinnavaia, T. J. Titanium-containing mesoporous molecular sieves for catalytic oxidation of aromatic compounds. *Nature* **368**, 321–323 (1994).
2. Ohkawa, H., Ohishi, N. & Yagi, K. Assay for lipid peroxides in animal tissues by thiobarbituric acid reaction. *Anal. Biochem.* **95**, 351–358 (1979).
3. Sishc, B. J., Ding, L., Nam, T. K., Heer, C. D. & Story, M. Avasopasem manganese synergizes with hypofractionated radiation to ablate tumors through the generation of hydrogen peroxide. *Sci. Transl. Med.* **13**, eabb3768 (2021).
4. Campos-Martin, J. M., Blanco-Brieva, G. & Fierro, J. Hydrogen peroxide synthesis: an outlook beyond the anthraquinone process. *Cheminform* **45**, 6962–6984 (2006).
5. Chung, T., Meshref, M., Hai, F. I., Al-Mamun, M. A. & Dhar, B. R. Microbial electrochemical systems for hydrogen peroxide synthesis: Critical review of process optimization, prospective environmental applications, and challenges. *Bioresour. Technol.* **313**, 123727 (2020).
6. Jennifer et al. Switching off hydrogen peroxide hydrogenation in the direct synthesis process. *Science* **323**, 1037–1041 (2009).
7. Dittmeyer, R., Grunwaldt, J. D. & Pashkova, A. A review of catalyst performance and novel reaction engineering concepts in direct synthesis of hydrogen peroxide. *Catal. Today* **248**, 149–159 (2015).
8. Perry, S. C., Pangotra, D., Vieira, L., Csepei, L. I. & Walsh, F. C. Electrochemical synthesis of hydrogen peroxide from water and oxygen. *Nat. Rev. Chem.* **3**, 442–458 (2019).
9. Siahrostami, S., Villegas, S. J., Mostaghimi, A., Back, S. & Montoya, J. H. A review on challenges and successes in atomic scale design of catalysts for electrochemical synthesis of hydrogen peroxide. *ACS Catal.* **10**, 7495–7511 (2020).
10. Lu, Z. et al. High-efficiency oxygen reduction to hydrogen peroxide catalysed by oxidized carbon materials. *Nat. Catal.* **1**, 156–162 (2018).
11. Jiang, K., Back, S., Akey, A. J., Xia, C. & Wang, H. Highly selective oxygen reduction to hydrogen peroxide on transition metal single atom coordination. *Nat. Commun.* **10**, 3997 (2019).
12. Zhang, Q., Zhou, M., Ren, G., Li, Y. & Du, X. Highly efficient electrosynthesis of hydrogen peroxide on a superhydrophobic three-phase interface by natural air diffusion. *Nat. Commun.* **11**, 1731 (2020).
13. Kim, H. W. et al. Efficient hydrogen peroxide generation using reduced graphene oxide-based oxygen reduction electrocatalysts. *Nat. catal.* **1**, 282–290 (2018).
14. Gao, J. & Liu, B. Progress of electrochemical hydrogen peroxide synthesis over single atom catalysts. *ACS Mater. Lett.* **2**, 1008–1024 (2020).
15. Fuku, K., Miyase, Y., Miseki, Y., Gunji, T. & Sayama, K. Enhanced oxidative hydrogen peroxide production on conducting glass anodes modified with metal oxides. *ChemistrySelect* **1**, 5721–5726 (2016).
16. Park, S. Y., Abroshan, H., Shi, X., Jung, H. S. & Zheng, X. CaSnO₃: An electrocatalyst for 2-electron water oxidation reaction to form H_2O_2. *ACS Energy Lett.* **4**, 352–357 (2018).
17. Kang, T. et al. Efficient hydrogen peroxide H_2O_2 synthesis by CaSnO₃ via two-electron water oxidation reaction. *ACS Sustain. Chem. Eng.* **8**, 15005–15012 (2020).
18. Kelly, S. et al. ZnO as an active and selective catalyst for electrochemical water oxidation to hydrogen peroxide. *Acs Catal.* **9**, 4593–4599 (2019).

19. Li, L., Hu, Z. & Yu, J. C. On-demand synthesis of H_2O_2 by water oxidation for sustainable resource production and organic pollutant degradation. *Angew. Chem. Int. Ed. Engl.* **59**, 20538–20544 (2020).

20. Mavrikis, S., Gltz, M., Rosiwal, S., Wang, L. & León, C. Boron-doped diamond electrocatalyst for enhanced anodic H_2O_2 production. *ACS Appl. Energy Mater.* **3**, 3169–3173 (2020).

21. Mavrikis, S., Perry, S. C., Leung, P. K., Wang, L. & Ponce de León, C. Recent advances in electrochemical water oxidation to produce hydrogen peroxide: a mechanistic perspective. *ACS Sustain. Chem. Eng.* **9**, 76–91 (2020).

22. Li, L. et al. Electrochemical generation ofhydrogen peroxide from a zinc gallium oxide anode with dual active sites. *Nat. Comm.* **14**, 1890 (2023).

23. Nadar, A. et al. Evaluating the reactivity of $BiVO_4$ surfaces for efficient electrocatalytic H_2O_2 production: A combined experimental and computational study. *J. Phys. Chem. C.* **124**, 4152–4161 (2020).

24. Jawad, A., Chen, Z. & Yin, G. Bicarbonate activation of hydrogen peroxide: a new emerging technology for wastewater treatment. *Chin. J. Catal.* **37**, 810–825 (2016).

25. Sablas, M. M. et al. Percarbonate mediated advanced oxidation completely degrades recalcitrant pesticide imidacloprid: Role of reactive oxygen species and transformation products. *Sep. Purif. Technol.* **250**, 117269 (2020).

26. Cao, Y., Cui, K., Chen, Y., Cui, M. & Yang, X. Efficient degradation of tetracycline by H_2O_2 catalyzed by FeOCl: A wide range of pH values from 3 to 7. *Solid State Sci.* **113**, 106548 (2021).

27. Fu, D. et al. Role of CuxO-Anchored Pyrolyzed Hydrochars on H_2O_2-Activated Degradation of Tetracycline: Effects of Pyrolysis Temperature and pH. *Ind. Eng. Chem. Res.* **61**, 8847–8857 (2022).

28. Wang, C. et al. Rapid degradation of norfloxacin by VUV/Fe^{2+}/H_2O_2 over a wide initial pH: Process parameters, synergistic mechanism, and influencing factors. *J. Hazard. Mater.* **416**, 125893 (2021).

29. Nie, Y., Hu, C., Qu, J., Zhou, L. & Hu, X. Photoassisted degradation of azodyes over FeOxH2x-3/Fe0 in the presence of H_2O_2 at neutral pH values. *Environ. Sci. Technol.* **41**, 4715 (2007).

30. Jiang, Z., Wang, L., Lei, J., Liu, Y. & Zhang, J. Photo-Fenton degradation of phenol by CdS/rGO/Fe^{2+} at natural pH with in situ-generated H_2O_2. *Appl. Catal. B* **241**, 367–374 (2018).

31. Ohsaki, Y. et al. Two-electron oxidation of water to form hydrogen peroxide initiated by one-electron oxidation of Tin (IV)-porphyrins. *J. Photochem. Photobiol. A* **401**, 112732 (2020).

32. Sebastian, A. et al. Protolytic behavior of water-soluble zinc(II) porphyrin and the electrocatalytic two-electron water oxidation to form hydrogen peroxide. *J. Photochem. Photobiol. A* **400**, 112619 (2020).

33. Xue, S. G. et al. Selective electrocatalytic water oxidation to Produce H_2O_2 Using a C,N Codoped TiO_2 electrode in an acidic electrolyte. *ACS Appl. Mater. Interfaces* **12**, 4423–4431 (2020).

34. Lai, Y. et al. Objective observations of the electrochemical production of H_2O_2 in $KHCO_3$ aqueous electrolyte and related application inspirations. *J. Phys. Chem. C.* **125**, 19831–19838 (2021).

35. Givan, A., Loewenschuss, A., Nielsen, C. J. & Rozenberg, M. FTIR and computational studies of pure and water containing SO_3 species in solid argon matrices. *J. Mol. Struct.* **830**, 21–34 (2007).

36. Haupa, K., Bil, A. & Mielke, Z. Donor–acceptor Complexes between ammonia and sulfur trioxide: An FTIR and computational study. *J. Phys. Chem. A* **119**, 10724–10734 (2015).

37. Schriver, L., Carrere, D., Schriver, A. & Jaeger, K. Matrix-isolation photolysis of SO_2, O_3 and H_2O: evidence for the H_2O: SO_3 complex. *Chem. phys. lett.* **181**, 505–511 (1991).

38. Pasquale, M. A. et al. A new polymeric [Cu(SO_3(CH_2)$_3$S–S(CH_2)$_3$$SO_3$)($H_2O$)$_4$]n complex molecule produced from constituents of a superconformational copper plating bath: Crystal structure, infrared and Raman spectra and thermal behaviour. *Solid State Sci.* **9**, 862–868 (2007).

39. Rozenberg, M., Loewenschuss, A. & Nielsen, C. J. H-Bonding of sulfuric acid with its decomposition products: An infrared matrix isolation and computational study of the $H_2SO_4 \cdot H_2O \cdot SO_3$ complex. *J. Phys. Chem. A* **120**, 3450–3455 (2016).

40. Steiger, M. & Asmussen, S. Crystallization of sodium sulfate phases in porous materials: The phase diagram Na_2SO_4–H_2O and the generation of stress. *Geochim. Cosmochim. Acta* **72**, 4291–4306 (2008).

41. Dong, J. L., Xiao, H. S., Zhao, L. J. & Zhang, Y. H. Spatially resolved Raman investigation on phase separations of mixed Na_2SO_4/$MgSO_4$ droplets. *J. Raman Spectrosc.* **40**, 338–343 (2009).

42. Jing, M., Jiang, L., Wang, S., Jing, F. & Sun, G. Application of FTIR in direct methanol fuel cells – Quantitative analysis of PTFE in gas diffusion layers. *Int. J. Hydrog. Energy* **38**, 7957–7963 (2013).

43. Murugavel Shanthi, P., Jampani Hanumantha, P., Albuquerque, T., Gattu, B. & Kumta, P. N. Novel composite polymer electrolytes (CPEs) of PVdF–HFP derived by electrospinning with enhanced Li-ion conductivities for rechargeable lithium – sulfur batteries. *ACS Appl. Energy Mater.* **1**, 483–494 (2018).

44. Elmar et al. Raman imaging with a fiber-coupled multichannel spectrograph. *Sensors* **14**, 21968–21980 (2014).

45. Yang, Z. et al. Role of sulfur trioxide (SO_3) in gas-pase elemental mercury immobilization by mineral sulfide. *Environ. Sci. Technol.* **53**, 3250–3257 (2019).

46. Smirnov, M. Y., Kalinkin, A. V., Pashis, A. V., Prosvirin, I. P. & Bukhtiyarov, V. I. Interaction of SO_2 with Pt model supported catalysts studied by XPS. *J. Phys. Chem. C.* **118**, 22120–22135 (2014).

47. Moulder J. F., Stickle W. F., Sobol P. E., Bomben K. D. Handbook of X-Ray Photoelectron Spectroscopy. *Chem. phys. lett.,* (Handbook of Chemistry and Physics, 92nd Ed., CRC. 1995).

48. Weaver, J. F. & Hoflund, G. B. Surface characterization study of the thermal decomposition of Ag_2O. *Chem. Mater.* **102**, 2263–2268 (1994).

49. Svintsitskiy, D. A., Kardash, T. Y. & Boronin, A. I. Surface dynamics of mixed silver-copper oxide $AgCuO_2$ during X-ray photoelectron spectroscopy study. *Appl. Surf. Sci.* **463**, 300–309 (2018).

50. Baggetto, L., Dudney, N. J. & Veith, G. M. Surface chemistry of metal oxide coated lithium manganese nickel oxide thin film cathodes studied by XPS. *Electrochim. Acta* **90**, 135–147 (2013).

51. Yuxin et al. Epitaxial growth of hyperbranched Cu/Cu_2O/CuO core-shell nanowire heterostructures for lithium-ion batteries. *Nano Res.* **8**, 2763–2776 (2015).

52. Nossol, E. et al. Synthesis, characterization and morphology of reduced graphene oxide–metal–TCNQ nanocomposites. *J. Mater. Chem. C.* **2**, 870–878 (2014).

53. Min et al. Oriented-assembly of hierarchical Fe_3O_4@$CuSiO_3$ microchains towards efficient separation of histidine-rich proteins. *Microporous Mesoporous Mater.* **286**, 207–213 (2019).

54. Hu, Z., Shen, Z., Yu, J. C. & Cheng, F. Intrinsic defect based homojunction: A novel quantum dots photoanode with enhanced charge transfer kinetics. *Appl. Catal. B.* **203**, 829–838 (2017).

55. Yang et al. Vertically aligned mixed V_2O_5-TiO_2 nanotube arrays for supercapacitor applications. *Chem. comm.* **47**, 7746–7748 (2011).

56. Miyase, Y., Iguchi, S., Miseki, Y., Gunji, T. & Sayama, K. Electrochemical H_2O_2 Production and Accumulation from H_2O by Composite Effect of Al_2O_3 and $BiVO_4$. *J. Electrochem. Soc.* **166**, H644–H649 (2019).

57. Fuku, K., Miyase, Y., Miseki, Y., Gunji, T. & Sayama, K. WO_3/$BiVO_4$ photoanode coated with mesoporous Al_2O_3 layer for oxidative production of hydrogen peroxide from water with high selectivity. *RSC Adv.* **7**, 47619–47623 (2017).

58. Gill, T. M., Vallez, L. & Zheng, X. The role of bicarbonate-based electrolytes in H_2O_2 production through two-electron water oxidation. *ACS Energy Lett.* **6**, 2854–2862 (2021).

59. Manor, J. & Arkin, I. T. Gaining insight into membrane protein structure using isotope-edited FTIR. *Biochimica et. Biophysica Acta (BBA) - Biomembranes* **1828**, 2256–2264 (2013).

60. Torres, J., Kukol, A., Goodman, J. M. & Arkin, I. T. Site-specific examination of secondary structure and orientation determination in membrane proteins: The peptidic C-13=O-18 group as a novel infrared probe. *Biopolymers* **59**, 396–401 (2015).

61. Torres, J., Adams, P. D. & Arkin, I. T. Use of a New Label, 13C 18O, in the determination of a structural model of phospholamban in a lipid bilayer. spatial restraints resolve the ambiguity arising from interpretations of mutagenesis data. *J. Mol. Biol.* **300**, 677–685 (2000).

62. Schmidt, M. & Lutz, H. D. Hydrogen bonding in basic copper salts: a spectroscopic study of malachite, Cu2(OH)2CO3, and brochantite, Cu4(OH)6SO4. *Phys. Chem. Miner.* **20**, 27–32 (1993).

63. Du, J. et al. Conversion of solid Cu2(OH)2CO3 into HKUST-1 metal-organic frameworks: Toward an under-liquid superamphiphobic surface. *Surf. Coat. Technol.* **363**, 282–290 (2019).

64. Hu, Z., Lu, Y., Liu, M., Zhang, X. & Cai, J. Crystalline red phosphorus for selective photocatalytic reduction of CO_2 into CO. *J. Mater. Chem. A* **9**, 338–348 (2021).

65. Hu, Z. F. et al. Cu(In,Ga)Se$_2$ for selective and efficient photo-electrochemical conversion of CO_2 into CO. *J. Catal.* **384**, 88–95 (2020).

66. Hu, Z. & Liu, W. Conversion of biomasses and copper into catalysts for photocatalytic CO_2 reduction. *ACS Appl. Mater. Inter.* **12**, 51366–51373 (2020).

67. Lan, Y., Niu, G., Wang, F., Cui, D. & Hu, Z. SnO$_2$-modified two-dimensional CuO for enhanced electrochemical reduction of CO_2 to C_2H_4. *ACS Appl. Mater. Interfaces* **12**, 36128–36136 (2020).

68. Bachhuber, F. et al. Van der Waals interactions in selected allotropes of phosphorus. *Z. Kristallogr. Cryst. Mater.* **230**, 107–115 (2015).

Acknowledgements

Author contributions

R. W. and Z. H. designed the experiments. R. W. conducted the experiments, performed testing, analyzed data, and drafted and revised the manuscript. H. Luo assisted with the experiments. H. L., C. D., H. Liu, M. S., Q. Z., Z. O., Y. L. and G. L. discussed the results and commented on the manuscript. J. Y. and Z. H. reviewed and revised the manuscript. Z.H. supervised the project.

Competing interests

The authors declare no competing interests.

Additional information

Supplementary information The online version contains supplementary material available at https://doi.org/10.1038/s41467-024-54593-4.

Correspondence and requests for materials should be addressed to Zhuofeng Hu.

Peer review information *Nature Communications* thanks the anonymous, reviewers for their contribution to the peer review of this work. A peer review file is available.

Reprints and permissions information is available at http://www.nature.com/reprints

Publisher's note Springer Nature remains neutral with regard to jurisdictional claims in published maps and institutional affiliations.